Journal of Innovative Optical Health Sciences
Vol. 4, No. 1 (2011) 73–78

DOI: 10.1142/S1793545811001265

IMAGE IMPROVEMENT IN THE WAVELET DOMAIN FOR OPTICAL COHERENCE TOMOGRAMS

YINGLI WANG, YANMEI LIANG*, JINGYI WANG and SHU ZHANG
Institute of Modern Optics, Nankai University
Key Laboratory of Opto-electronic Information Science and Technology
Education Ministry of China, Tianjin 300071, China
**ymliang@nankai.edu.cn*

In this paper, an image processing method for improving the quality of optical coherence tomography (OCT) images is proposed. Wavelet denoising based on context modeling and contrast enhancement by means of the contrast measure in the wavelet domain is carried out on the OCT images in succession. Three parameters are selected to assess the effectiveness of the method. It is shown from the results that the proposed method can not only enhance the contrast of images, but also improve signal-to-noise ratio. Compared with two other typical algorithms, it has the best visual effect.

Keywords: Optical coherence tomography; noise in imaging systems; image enhancement; wavelets.

1. Introduction

Optical Coherence Tomography (OCT) is a promising technology that can be applied to obtain high-resolution microstructure images of biological tissues.[1–4] However, because of scattering and absorption, especially for the high-scattering specimen, not only the incident light is rapidly attenuated with it propagating into the tissue, but also the backscattering light from the internal structure is attenuated with it propagating out of the tissue, which makes the backscattering light from the deep tissue have much lower intensity than that of the surface of the tissue. In addition, the basic human visual properties of insensitive to low gray-level pixels make it challenging to distinguish the exact internal details of specimen for the unprocessed OCT images due to a relatively low contrast in the deeper internal tissue. Meanwhile, multiple kinds of noise during OCT signal collecting process also reduce the visibility in the deep tissue. Much work has been done to enhance the contrast of OCT images, of which the most common ways are logarithmic transform, histogram matching, and other quantization methods in the spatial domain.[5,6] These quantization methods apply the enhancement algorithm to all the pixels of the images simultaneously, which may enhance the noise in the OCT images when amplifying the signal. Therefore, suppressing the noise before image enhancement is especially essential. Denoising methods in OCT images reported include Rotating Kernel Transformation,[7] I-divergence regularization,[8] and digital filtering,[9] such as the enhanced Lee filter, median filter, the symmetric nearest neighbor filter, the adaptive Wiener filter, etc. Among all the

*Corresponding author.

denoising methods, filtering in the wavelet domain[10] is regarded as the quite effective one.

In this paper, we propose a method of image improvement in wavelet domain, in which a noise reduction algorithm is applied before contrast enhancement to suppress noise. Unlike enhancement techniques in the spatial domain, wavelet-based algorithms offer the capability of enhancing image components adaptively based on their spatial-frequency properties. The method contains adaptive wavelet denoising method based on context modeling[11] and contrast enhancement method by means of the contrast measure in the wavelet domain.[12] Compared with histogram matching and the deconvolution method by Wiener filter, it is demonstrated that the adaptive image improvement method can not only suppress the noise in the image, but also enhance the image contrast to make it have better visual quality.

2. Method

Wavelet transform has been widely employed in different applications including signal processing and image processing in the past years. The advantages of wavelet-based methods lie in that it can decompose the signal into different subbands by wavelet transform so that one can process the signals in the different subbands with an appropriate method in the wavelet domain, while ignoring or reducing the contribution of other subbands.

In the spatial domain, a degraded image $g(x, y)$ can be modeled as

$$g(x, y) = f(x, y) + n(x, y), \tag{1}$$

where $f(x, y)$ and $n(x, y)$ are the original or noise-free image and noise, respectively. When a degraded OCT image $g(x, y)$ is transformed into the wavelet domain, its wavelet coefficients $w(i, j)$ of different levels can be calculated by an appropriate wavelet filter. Horizontal, vertical, and diagonal details are separated into the high-frequency subbands HL_m, LH_m, and HH_m, whose coefficients are correspondingly represented by $D_m^k(i, j)$ $(k = 1, 2, 3)$, respectively, and m is the decomposition level. Approximation coefficients in the low-frequency subband can be expressed as $A_m(i, j)$. Therefore, for the degraded image, in the wavelet domain, its wavelet coefficients at the mth level can be given as

$$w_m^{(o)}(i, j) = y_m^{(o)}(i, j) + v_m^{(o)}(i, j), \tag{2}$$

where $w_m^{(o)}(i, j)$ are the observed coefficients, $y_m^{(o)}(i, j)$ are unknown noise-free coefficients, $v_m^{(o)}(i, j)$ are noise coefficients, $o \in \{LL, HL, LH, HH\}$ is the subband orientation. Modular square wavelet threshold is applied to each $w_m^{(o)}(i, j)$ in all the high-frequency subbands to approximate to $y_m^{(o)}(i, j)$, and the denoised coefficients $\bar{w}_m^{(o)}(i, j)$ are obtained by

$$\bar{w}_m^{(o)}(i, j) = \begin{cases} \operatorname{sgn}(w_m^{(o)}(i, j)) \sqrt{\left[\left(w_m^{(o)}(i, j)\right)^2 - \left(T_m^{(o)}(i, j)\right)^2\right]}, & \left| w_m^{(o)}(i, j) \right| \geq T_m^{(o)}(i, j), \\ 0, & \left| w_m^{(o)}(i, j) \right| < T_m^{(o)}(i, j), \end{cases} \tag{3}$$

where sgn represents the signum function, and the threshold $T_m^{(o)}(i, j)$ at the location (i_0, j_0) can be calculated by the formula

$$T_m^{(o)}(i_0, j_0) = \frac{\sigma_n^2}{\sigma_X(i_0, j_0)}, \tag{4}$$

and σ_n, σ_X are the standard deviations of the noise and the signal, respectively. σ_n can be estimated by using the robust median estimator in the highest subband HH_1 of the wavelet transform,

$$\sigma_n = \frac{\text{Median}(|w(i, j)|)}{0.6745}, \quad w(i, j) \in \text{subband } HH_1, \tag{5}$$

and the estimation of $\sigma_X^2(i_0, j_0)$ is[11]

$$\sigma_X^2(i_0, j_0) = \max\left(\frac{1}{2L+1} \sum_{[k,l] \in B_{i_0 j_0}} w_m(k, l)^2 - \sigma_n^2, 0\right), \tag{6}$$

where $B_{i_0 j_0}$ denotes a set of points whose context falls in a moving window. The moving window is selected from the matrix of the context of all points in a subband of the mth level with $P_m \times Q_m$ wavelet coefficients, and point (i_0, j_0) is just located in the center of the moving window with a width of $2L + 1$. $L = \max(50, 0.02 P_m Q_m)$ is chosen to ensure that enough points are used to estimate the variance $\sigma_X^2(i_0, j_0)$. Therefore, the threshold can be calculated according to the image itself to make the denoising method adaptive to different images.

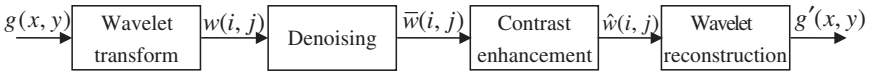

Fig. 1. The flowchart of the method.

After processing the wavelet coefficients to reduce the noise, a contrast enhancement algorithm is applied to improve the signal of internal tissue. In the algorithm, a parameter of contrast measure at the mth level in wavelet domain is defined as[13]

$$\bar{C}^k_m(i,j) = \frac{\bar{D}^k_m(i,j)}{\bar{A}_m(i,j)}, \tag{7}$$

where $\bar{D}^k_m(i,j)$ and $\bar{A}_m(i,j)$ are the denoising wavelet coefficients in the high-frequency subbands and in the low-frequency subbands at the mth level, respectively. If the image enhancement control factors are supposed to be $\lambda^k_m(i,j)$, the contrast of the enhanced image $\hat{C}^k_m(i,j)$ can be described as

$$\hat{C}^k_m(i,j) = \lambda^k_m(i,j)\bar{C}^k_m(i,j). \tag{8}$$

Under the hypothesis that all the image enhancement control factors in one decomposition level are identical ($\lambda^k_m(i,j) = \lambda_m$), we use the enhancement equation,[12]

$$\hat{D}^k_m(i,j) = \lambda_m \frac{\hat{A}_m(i,j)}{\bar{A}_m(i,j)} \bar{D}^k_m(i,j)$$

$$= \lambda_m \frac{\hat{E}_{L_m}}{\bar{E}_{L_m}} \bar{D}^k_m(i,j), \tag{9}$$

where $\hat{D}^k_m(i,j)$ and $\hat{A}_m(i,j)$ are the enhanced wavelet coefficients in the high-frequency subbands and in the low-frequency subbands at the mth level, respectively. $\bar{E}_{L_m} = [\sum\sum \bar{A}_m(i,j)]/(P_m \times Q_m)$ is the intensity mean in low-frequency subband which contains $P_m \times Q_m$ coefficients, and $\hat{E}_{L_m}$ can be calculated as[14]

$$\hat{E}_{L_m} = 65 + \beta\bar{E}_{L_m}. \tag{10}$$

Finally, utilize the enhanced coefficients of all levels $\hat{D}^k(i,j)$ and $\hat{A}(i,j)$ to reconstruct the processed image by inverse wavelet transform.

The total proposed method can be summarized as follows:

(1) Project $g(x,y)$ into the wavelet domain with M levels to obtain the degraded wavelet coefficients $w(i,j)$ in each subband. Let $m = M$.
(2) Obtain the denoising wavelet coefficients $\bar{w}^{(o)}_m(i,j)$ in the mth decomposition level according to Eqs. (3)–(6).
(3) Calculate the intensity mean in the low-frequency subbands $\bar{E}_{L_m}$ and obtain the enhanced intensity mean $\hat{E}_{L_m}$ according to Eq. (10).
(4) Get $\hat{D}^k_m(i,j)$ according to Eq. (9). Remain $\bar{A}_m(i,j)$, which means $\hat{A}_m(i,j) = \bar{A}_m(i,j)$.
(5) Utilize the $\hat{D}^k_m(i,j)$ and $\hat{A}_m(i,j)$ to calculate the enhanced low-resolution residual of the $(m-1)$th level, $\hat{A}_{m-1}(i,j)$, by inverse wavelet transform.
(6) Let $m = m - 1$, and repeat (2)–(5) to calculate the low-resolution residuals of all the decomposition levels until $m = 1$ to obtain $\hat{A}_0(i,j)$, which is the processed image $g'(x,y)$.

In short, the whole method is decomposing the degraded image $g(x,y)$ into different levels by wavelet transform, after denoising and contrast enhancement in the wavelet domain, then executing inverse wavelet transform to reconstruct the improved image. The flowchart of the method is shown in Fig. 1.

3. Results

To demonstrate the feasibility of the method, the images obtained from a time-domain OCT system are processed. For comparison, after reducing the noise for OCT images by the noise reduction algorithm in the wavelet domain, deconvolution method by Wiener filter and histogram matching method are also applied to the denoising images. The wavelet function used for wavelet transformation in this paper is the near-symmetric symmlet 4-tap wavelet and 4-level 2D wavelet decomposition is done. Figures 2(a)–2(d) show the original OCT image of the orange tissue, the deconvolution result by Wiener filter, the result of histogram matching, and the result of our method, respectively. The enhancement factors λ and β used in the orange image are 1.5 and 1.8, respectively. It can be seen that all the processed images have better visual effect, while Fig. 2(d) has the best contrast which

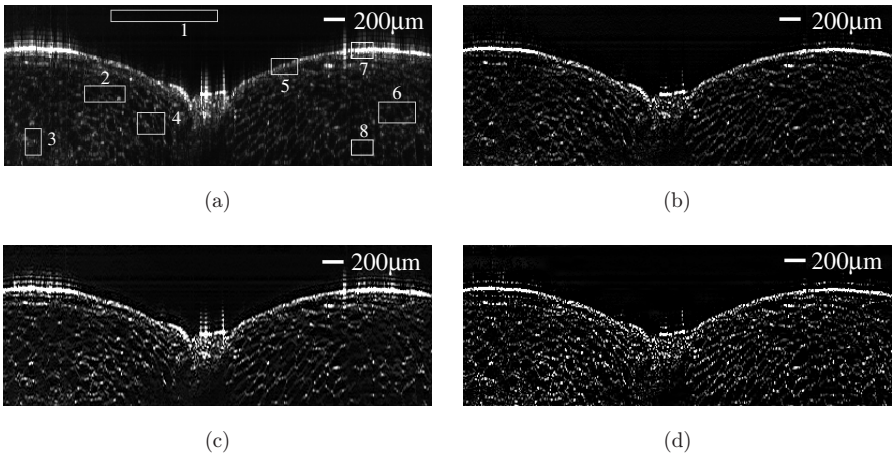

Fig. 2. The OCT images of orange pulp tissue. (a) The original OCT image. (b)−(d) The images processed by histogram matching, deconvolution with Wiener filter, and the proposed method, respectively.

makes the internal structure details of the pulp be seen much more clearly.

Signal-to-noise ratio (SNR), region contrast (RC), and regions' intensity ratio (RIR) are selected to evaluate the effectiveness of denoising, edge enhancement, and the internal image enhancement of the above algorithms, respectively. The SNR is calculated as follows:

$$\mathrm{SNR} = 10\log_{10}[\max(X_s)^2/\sigma_b^2], \tag{11}$$

where $\max(X_s)$ and σ_b^2 represent the average of the maximum gray value of each column and the variance of the background noise in the OCT image on a linear intensity scale, respectively.

RC can be calculated as in Ref. 13:

$$C_r = \frac{1}{N}\sum |c(x,y)|\log(1+|c(x,y)|), \tag{12}$$

where $c(x,y)$, the local contrast at point (x,y), is defined as

$$\begin{aligned} c(x,y) = {} & 4g(x,y) - \{g(x-1,y) + g(x,y-1) \\ & + g(x+1,y) + g(x,y+1)\}, \end{aligned} \tag{13}$$

$g(x,y)$ is the gray value of point (x, y) in the image, r represents a certain region of the image, and N is the total number of pixels in region r.

RIR is defined as the ratio of the signal intensity in the internal tissue to that of the surface, which can be expressed as

$$\mathrm{RIR} = \frac{\frac{1}{N_1}\sum_{x,y\in\mathrm{internal}} g(x,y)}{\frac{1}{N_2}\sum_{x,y\in\mathrm{surface}} g(x,y)}, \tag{14}$$

Table 1. Evaluated results of three aspects of images in Fig. 2.

	Fig. 2(a)	Fig. 2(b)	Fig. 2(c)	Fig. 2(d)
SNR (dB)	41.76	42.27	39.54	49.48
RC	2.47	6.42	6.31	15.92
RIR	0.25	0.28	0.26	0.44

where N_1 and N_2 are the number of pixels in the internal and surface regions, respectively. The higher the RIR is, the better the enhanced internal detail is.

Region 1 marked in Fig. 2(a) represents the background whose intensity is used to calculate σ_b^2, and regions 2−8 are regarded as the sample areas. The calculated results of the above three evaluating parameters of Figs. 2(a)−2(d) are shown in Table 1. The RC of each image is the average value of the RCs in regions 2−6. Regions 7 and 8 stand for the surface and the internal tissue, respectively, and the RIR is calculated by them. The SNR, RC, and RIR of all processed images in Fig. 2 are improved, except the SNR in Fig. 2(c). The SNR and RC of the image processed by the proposed method can reach up to 49.48 dB and 15.92 from 41.76 dB and 2.47 of the unprocessed image, respectively, which are obviously much higher than those of other images (42.27 dB and 6.42 by the histogram matching method, 39.54 dB and 6.31 by the deconvolution method). The improvement of RIR from 0.25 to 0.44 by our method illustrates that the internal signal are obviously enhanced.

Another OCT unprocessed and enhanced images of the skin of hoptoad are shown in Fig. 3, and the

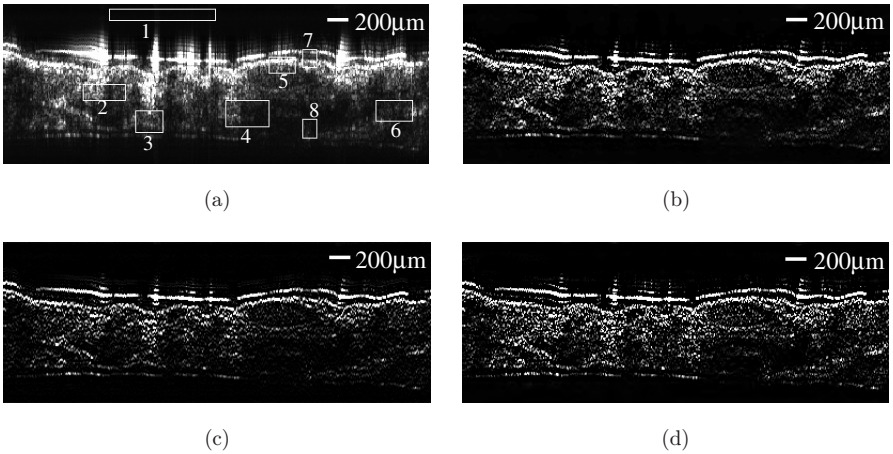

Fig. 3. The OCT images of hoptoad skin. (a) The original OCT image. (b)−(d) The images processed by histogram matching, deconvolution with Wiener filter, and our proposed method, respectively.

Table 2. Evaluated results of three aspects of images in Fig. 3.

	Fig. 3(a)	Fig. 3(b)	Fig. 3(c)	Fig. 3(d)
SNR (dB)	42.48	45.11	44.59	49.92
RC	1.96	8.25	8.02	14.37
RIR	0.27	0.28	0.29	0.32

calculated results of the evaluating parameters of these images are shown in Table 2. Compared with 42.48 dB and 1.96 in the unprocessed image (shown in Fig. 3(a)), the SNR and RC are increased to 49.92 dB and 14.37 by using the proposed method (shown in Fig. 3(d)), respectively. The histogram matching method (shown in Fig. 3(b)) can only provide about 45.11 dB in SNR and 8.25 in RC, and the values by using the deconvolution method (shown in Fig. 3(c)) is only about 44.59 dB and 8.02. The RIR also has an improvement from 0.27 to 0.32 by the proposed method. The enhancement factors λ and β used here are 1.6 and 1.5, respectively.

4. Discussion

From the above results, we can see that by using the noise reduction and contrast enhancement algorithm in succession, the SNR of the OCT images of orange pulp tissue and hoptoad skin can be increased by 7.72 dB and 7.44 dB, respectively. The RC of the OCT images of orange pulp tissue and hoptoad skin can be increased more than fivefold and sixfold. The improvement of the SNR and RC demonstrates that the proposed method can enhance the edge and keep the sharpness of the image besides denoising. The increase of RIR proves that the proposed method can enhance the internal depth information.

It is worth noting that the enhancement factors λ and β, which are used to adjust the contrast and the global dynamic range of the image, respectively, play a crucial role in the enhancement algorithm. They are chosen by experience, which are evaluated by the visual effect at first. It is shown from the experimental results that λ and β should be in the range of $1-2$ for the purpose of getting optimal visual effect. If they are smaller than 1, there will be no obvious enhancement in the processed image, whereas the larger value (>2) will lead the entire image to be extremely bright and the high gray values to be compressed. For simplifying calculation and reducing complexity, the same λ and β are applied to each level in this study. The suitable value of λ and β for each image which makes the algorithm adaptive is worth paying more attention in further research.

The spectrum of the light source applied in OCT, including superluminescent light-emitting diodes (SLD), amplified spontaneous emission (ASE), swept light source, etc., is usually non-Gaussian or not smooth; so the point response in the interferogram will have sidelobes, which may affect the processed results. A sidelobe suppression algorithm[15] can be used to preprocess the images if there are significant sidelobes in the images.

In the above wavelet-based contrast enhancement algorithm, the detailed coefficients are

amplified while the approximation coefficients remain the same. When being transformed into the wavelet domain, the edges of tissues with obvious structures are separated into the high-frequency subbands, so they can be enhanced. For the tissues with single structure or small refractive index gradient, their gray values for the continuous pixels in the OCT image are close to each other or have little changes, so they are mainly separated into the low-frequency subbands when being transformed into the wavelet domain and cannot be enhanced. Therefore, the method has better effect on OCT images which have obvious structure variation, such as cells and tissues with sandwich structure.

5. Conclusion

An image improvement method in the wavelet domain has been proposed to improve the quality of OCT images. The processed OCT images of orange pulp tissue and hoptoad skin demonstrate that our method can improve the visual effect better than two other typical methods. The improvement of SNR, RC, and RIR shows that the method can achieve the goals of noise reduction and contrast enhancement simultaneously.

Acknowledgments

This research is supported by the National Natural Science Foundation of China (Grant Nos. 60637020 and 60677012) and the Tianjin Foundation of Natural Science (No. 09JCZDJC18300).

References

1. D. Huang, E. A. Swanson, C. P. Lin, J. S. Schuman, W. G. Stinson, W. Chang, M. R. Hee, T. Flotte, K. Gregory, C. A. Puliafito, J. G. Fujimoto, "Optical coherence tomography," *Science* **254**(5035), 1178–1181 (1991).
2. M. Ruggeri, H. Wehbe, G. Tsechpenakis, S. Jiao, M. E. Jockovich, C. Cebulla, E. Hernandez, T. G. Murray, C. A. Puliafito, "Quantitative evaluation of retinal tumor volume in mouse model of retinoblastoma by using ultra high-resolution optical coherence tomography," *J. Innov. Opt. Health Sci.* **1**(1), 17–28 (2008).
3. Z. Yuan, H. Ren, W. Waltzer, J. Kim, J. Liu, K. Jia, H. Xie, Y. Pan, "Optical coherence tomography for bladder cancer diagnosis: from animal study to clinical diagnosis," *J. Innov. Opt. Health Sci.* **1**(1), 125–140 (2008).
4. M. Todorovic, S. Jiao, G. Stoica, L. V. Wang, "Preliminary study on skin cancer detection in sencar mice using Mueller optical coherence tomography," *J. Innov. Opt. Health Sci.* **2**(3), 289–294 (2009).
5. K. Yu, L. Ji, L. Wang, P. Xue, "How to optimize the OCT image," *Opt. Exp.* **9**(1), 24–35 (2001).
6. Y. Liu, Y. Liang, Z. Tong, X. Zhu, G. Mu, "Contrast enhancement of optical coherence tomography images using least squares fitting and histogram matching," *Opt. Comm.* **279**, 23–26 (2007).
7. J. Rogowska, M. E. Brezinski, "Evaluation of the adaptive speckle suppression filter for coronary optical coherence tomography imaging," *IEEE Trans. Med. Imaging* **19**(12), 1261–1266 (2000).
8. D. L. Marks, T. S. Ralston, S. A. Boppart, "Speckle reduction by I-divergence regularization in optical coherence tomography," *J. Opt. Soc. Am. A* **22**(11), 2366–2371 (2005).
9. A. Ozcan, A. Bilenca, A. E. Desjardins, B. E. Bouma, G. J. Tearney, "Speckle reduction in optical coherence tomography images using digital filtering," *J. Opt. Soc. Am. A* **24**(7), 1901–1910 (2007).
10. D. C. Adler, T. H. Ko, J. G. Fujimoto, "Speckle reduction in optical coherence tomography images by use of a spatially adaptive wavelet filter," *Opt. Lett.* **29**(24), 2878–2880 (2004).
11. S. G. Chang, B. Yu, M. Vetterli, "Spatially adaptive wavelet thresholding with context modeling for image denoising," *IEEE Trans. Image Process.* **9**(9), 1522–1531 (2000).
12. J. Tang, Q. Sun, K. Agyepong, "An image enhancement algorithm based on contrast measure in the wavelet domain for screening mammograms," *IEEE Int. Conf. Image Process.* **5**, 29–32 (2007).
13. J. Tang, X. Liu, Q. Sun, "A direct image contrast enhancement algorithm in the wavelet domain for screening mammograms," *IEEE J. Select. Topics Signal Process.* **3**(1), 74–80 (2009).
14. T. Peli, J. S. Lim, "Adaptive filtering for image enhancement," *Opt. Eng.* **21**(1), 108–112 (1982).
15. Y. Wang, Y. Liang, K. Xu, "Signal processing for sidelobe suppression in optical coherence tomography images," *J. Opt. Soc. Am. A* **27**(3), 415–421 (2010).